applied sciences

MDPI

Article

A New Technique for Determining the Shape of a Paper Sample in In-Plane Compression Test Using Image Sequence Analysis

Paweł Pełczyński [1,*], Włodzimierz Szewczyk [1], Maria Bieńkowska [1] and Zbigniew Kołakowski [2]

[1] Centre of Papermaking and Printing, Lodz University of Technology, Wólczańska 221, 95-003 Łódź, Poland
[2] Department of Strength of Materials, Lodz University of Technology, Stefanowskiego 1/15, 90-537 Łódź, Poland
* Correspondence: pawel.pelczynski@p.lodz.pl; Tel.: +48-426313816

Abstract: The article presents a new technique for analyzing phenomena occurring during the measurement of the strength properties of paper in the conditions of compression of the tested samples with forces acting in the paper plane. The technique is based on collecting data on the current distance of the clamps holding the tested sample and the force exerted on the sample using a universal testing machine and on the simultaneous recording of image sequence of the sample during the measurement. Next, the resulting images are subjected to processing and analysis, the purpose of which is to extract information about the shape of the sample edge in all phases of the measurement. Its advantage is the ability to determine the deflection arrow of the sample and describe its shape using the selected function given by the analytical parametric formula. It will be helpful in further research on the development of an analytical model describing the phenomena occurring during paper compression, and a method to determine the mechanism of paper destruction and the corresponding maximum force that destroys a paper sample.

Keywords: strength properties of paper; analysis of digital images; modelling of the shape of a paper sample; deflection arrow

Citation: Pełczyński, P.; Szewczyk, W.; Bieńkowska, M.; Kołakowski, Z. A New Technique for Determining the Shape of a Paper Sample in In-Plane Compression Test Using Image Sequence Analysis. *Appl. Sci.* **2023**, *13*, 1389. https://doi.org/10.3390/app13031389

Academic Editor: Milena Pavlíková

Received: 21 December 2022
Revised: 11 January 2023
Accepted: 16 January 2023
Published: 20 January 2023

1. Introduction

Paper is an orthotropic material commonly used for the production of corrugated and cellular cardboard, from which a variety of packaging is then produced [1,2]. Their usefulness is determined by the strength properties, which depend to a large extent on the properties of the paper itself [3–9]. At the same time, it is desirable to minimize the weight of the package while maintaining the required strength. In order to avoid time-consuming, experimental selection of the material composition of the cardboard from which the packaging is made, it is increasingly used to predict their strength properties by means of calculations that take into account the properties of the papers used in their production [10–14]. One of the important properties is the resistance to edge crushing measured in the compression test at short fastening—SCT [15]. Due to the orthotropy of the paper, resistance to crushing is determined in two main directions, namely MD (machine direction) and CD (cross direction).

However, the test does not take into account the phenomenon of buckling of the tested sample, which occurs when using longer sample attachment lengths and is commonly observed in corrugated cardboard packaging. Analysis of the compressive strength of various materials in the buckling state has been of interest to researchers for many years because it is of great importance for estimating the load capacity of mechanical structures [16–19]. However, the study of paper properties in this area was usually limited to simple compression tests and was not combined with simultaneous observation of the shape of the compressed samples.

Modern methods of processing and analyzing digital images make it possible to observe changes in the shape of bodies subjected to external forces on the basis of the

analysis of their series of images [20,21]. Thanks to advances in electronics, it is now possible to record sequences of images of processes occurring during strength tests of various materials in real-time. The series of images obtained in this way can be reviewed in any way, focusing on the significant phenomena occurring during the experiment, and can also be subjected to automatic analysis, the purpose of which is a quantitative description of a given process. An example of such a solution is the Lenso vision system for recording the surface of materials subjected to mechanical testing. Thanks to the use of Digital Image Correlation [22,23] in the square areas of successive images in the sequence, they allow for precise estimation of local deformations of the observed surfaces. Vision systems are also used in papermaking and printing to detect defects and assess the quality of produced paper or print [24]. This is possible thanks to the use of advanced algorithms for detecting defects visible in subsequent images of the recorded sequence, and often also algorithms for automatic recognition of the type of defect. Implementation of these operations in real time requires the use of computers with high computing power. This allows to control the production line based on the information received and improve the parameters of the production process or reject a defective product.

Observing the shape of paper samples during the crushing resistance test allows for associating changes in the shape of the sample with the magnitude of the force acting on it during the test. To make this possible, it is necessary to record images of the sample being tested and synchronize the resulting series of images with data from the machine.

2. Materials and Methods

2.1. Measuring Setup

The use of digital image analysis methods in measuring the crushing resistance of paper required solving the problem of synchronization of measurement in a universal testing machine with the recording of images of the tested samples. In order to simultaneously record the displacement of the moving handle of the testing machine and the force acting on the compressed sample and the images of the sample to be tested, the measuring setup shown in Figure 1a was prepared.

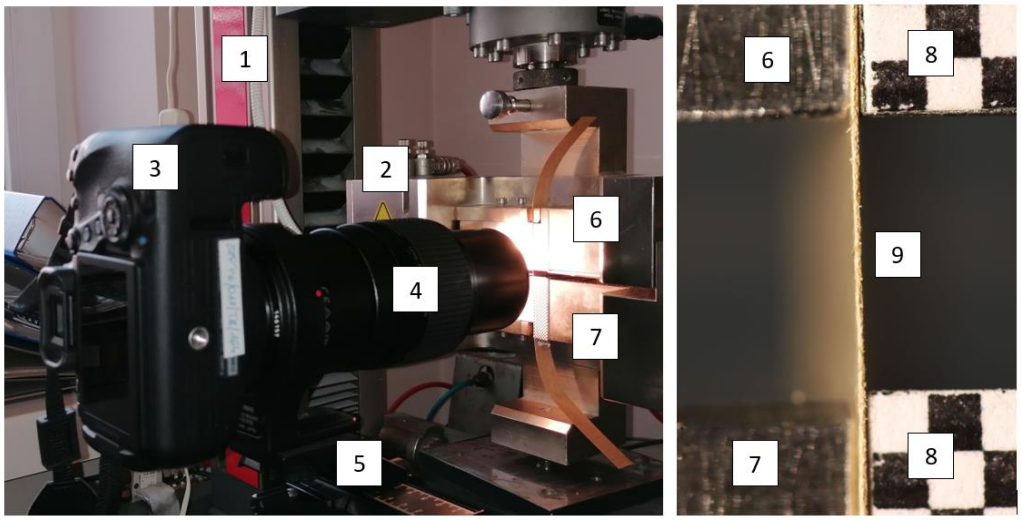

(**a**) (**b**)

Figure 1. View of (**a**) the measuring station, (**b**) the handles of the testing machine with sticked checkerboard patterns and the paper sample to be tested.

The stand consists of a testing machine (1) Zwick Roell Z 010, an SCT test holder (2), a camera placed on a tripod (3)—a Canon EOS 6D Mark II full-frame DSLR with a Canon MP-E 65 mm f/2.8 1–5 × Macro lens (4) and an illuminator providing constant illumination with the possibility of adjusting its direction (not visible in the photo). This

allows to achieve good contrast between the edge of the paper sample under examination and the background. In order to adjust the sharpness of the image, the camera is attached to the tripod via a setting sledge (5). This makes it possible to adjust the position of the camera in two horizontal axes—parallel and perpendicular to the optical axis of the camera. The camera lens allows to manually change the scale of reproduction in the range of 1 to 5, which gives the size of the recorded fragment of the paper sample in the range of 7.2 mm × 5.8 mm to 36 mm × 24 mm. In the prepared measuring setup, magnifications in the range of 4 to 5 were used.

Patterns of checkerboard (8) with a length of a single square of 1 mm (Figure 1b) were sticked to the fixed (6) and movable (7) clamps of the testing machine. It allowed to track the movement of the handle (6) and to determine the spatial resolution of the recorded images.

The measurement begins by placing the tested paper sample (9) in the SCT holders of the testing machine, setting the desired focal length of the lens and positioning the camera in such a way that the sample and the checkerboard fragments containing at least two intersections between its fields are in the field of vision. Next, the force value is reset, the recording of the sequence of photos is started and after recording 3–4 images, the measurement is initiated in the machine. The measurement ends when the set displacement of the movable handle is reached. During the entire measurement, a recording of the sequence of images of the sample is performed along with fragments of handles with sticked checkerboards.

2.2. A Sequence of Operations Included in the Developed Measurement Technique

The developed measurement technique consists of a series of operations that must be performed in order to obtain correct measurement results and their analysis. The flow diagram of the entire measurement is shown in Figure 2. The tested material and processed data are presented in the figure by means of gray rectangles. Operations included in the measurement process are shown in light blue rectangles with rounded corners.

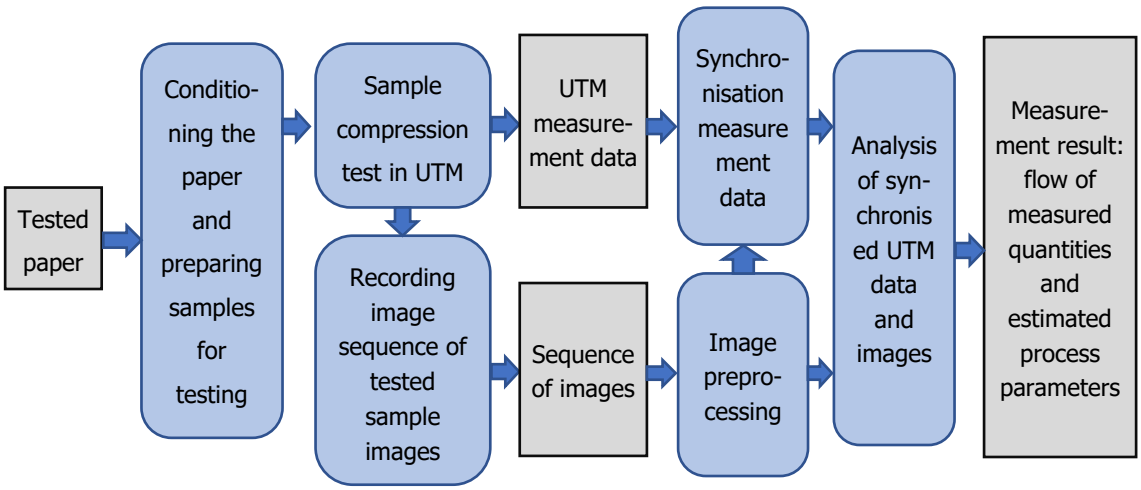

Figure 2. Flow diagram of the entire measurement procedure.

2.3. Developed Image Processing and Analysis Technique

The recorded sequence of images was subjected to pre-processing and analysis. Pre-processing consisted of the following stages:

- conversion of a series of RAW images to TIFF format with optional reducing the size of a digital image to reduce data volume,
- extracting information about the recording time of each photo in the sequence with an accuracy of 1/100 of a second,
- conversion of color images to grayscale,

- cropping obtained images to the following regions: the examined paper sample, the checkerboard on the movable handle, and the checkerboard on the fixed handle,
- linear filtering of the sample image by means of a filter that enhances the vertical edges in the image; its mask is shown in Figure 3,
- linear filtering of checkerboard images using a filter that emphasizes the corners of the checkerboard fields in the image; its mask is shown in Figure 4.

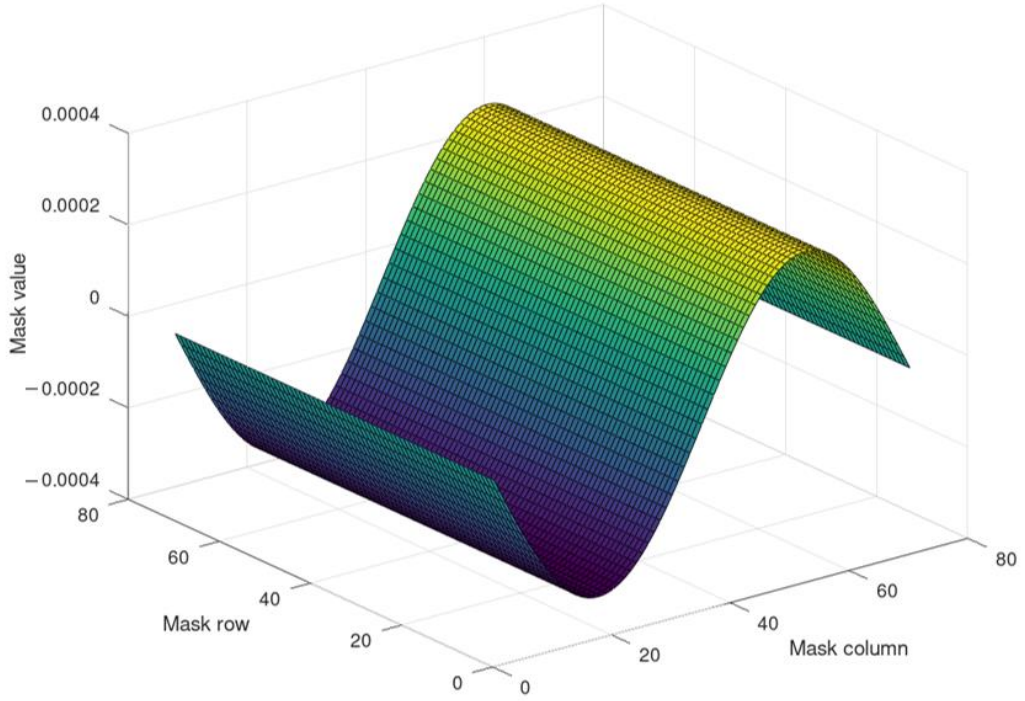

Figure 3. Filter mask designed to emphasize edges in an image.

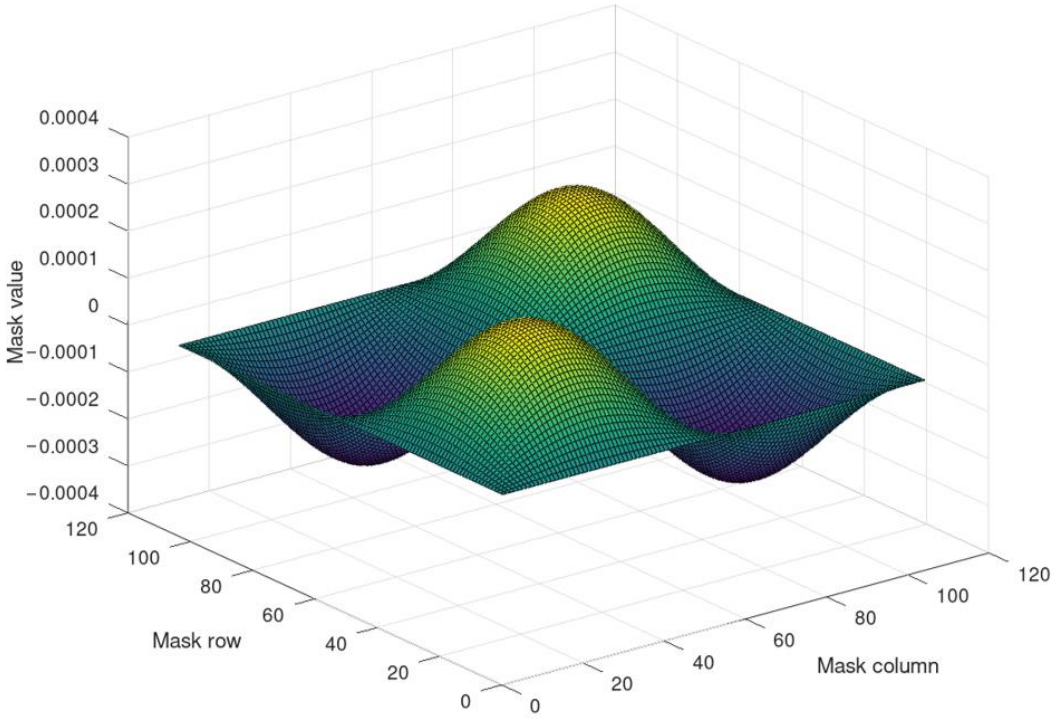

Figure 4. Filter mask designed to emphasize checkerboard corners in an image.

The results of filtering the sample image are shown in Figure 5a. Figure 5b shows the image of the sample itself with the detected edges of the sample: left (green) and right (red). Detecting the left edge is very difficult due to the low contrast in the image, hence in further analysis it was decided to rely on the detection of the right edge. This cannot be generalized to all cases. The contrast depends on the direction and lighting of the sample. In the future, choosing the right filter mask should be an option for the analysis algorithm.

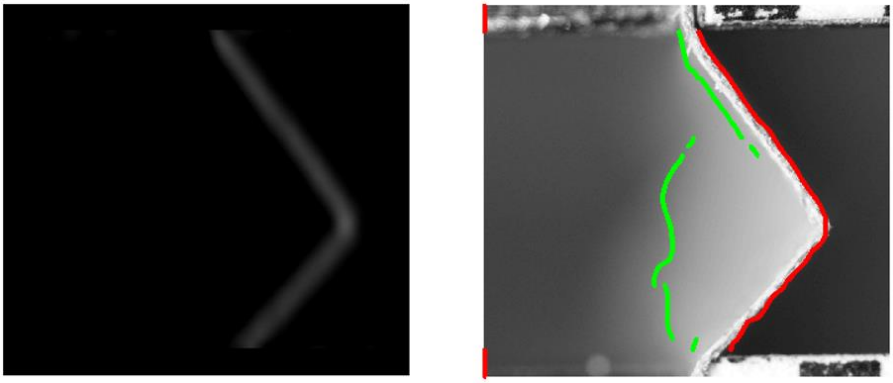

(**a**) (**b**)

Figure 5. (**a**) The result of filtering the image of the paper sample during the measurement, (**b**) the image of the sample with the detected left edge marked in green and the right edge in red.

Figure 6 shows the result of filtering the checkerboard images placed on both handles of the testing machine and the places where the corners marked with red dots were detected. To detect the corners between the white and black fields, regardless of their order, filtering was repeated twice with the filter mask rotated 90 degrees. Next, in the obtained images, the places of the corners were detected independently by detecting the maxima in the images after the filtering and the resulting information from both images was combined.

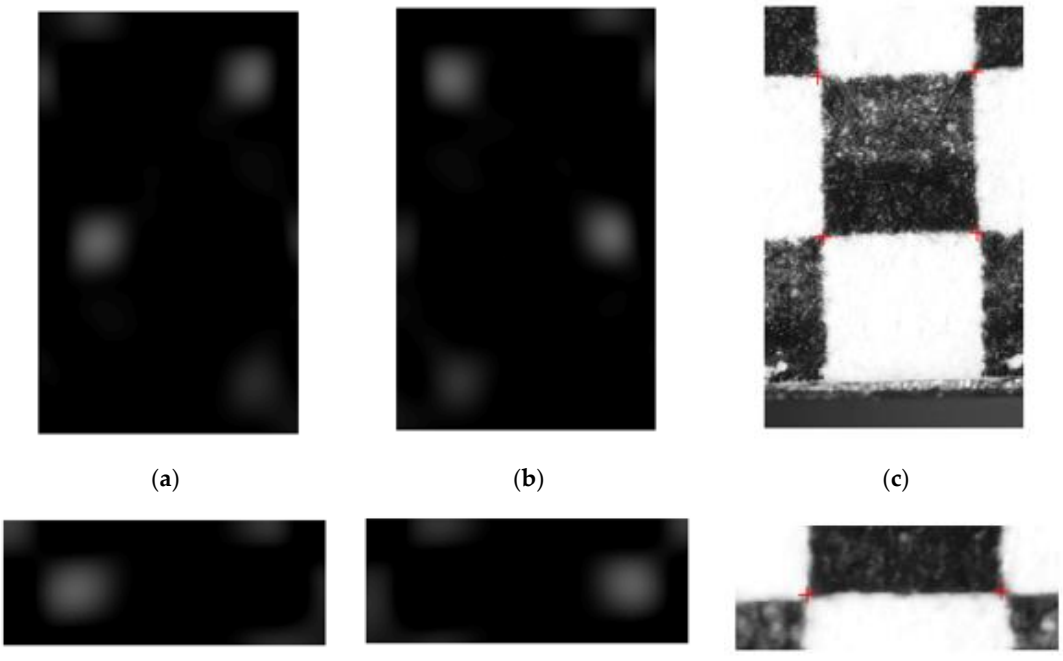

(**a**) (**b**) (**c**)

(**d**) (**e**) (**f**)

Figure 6. The result of filtering the checkerboard image on the moving (**a**,**b**) and still (**d**,**e**) handle and images of the handles themselves (**c**,**f**) with the corner detection points marked in red. Pictures (**b**,**e**) show the result of filtering with a filter with a mask rotated by 90°.

The coordinate sets of the points of the detected edges and corners were input information to the algorithm for the analysis of image data. The image coordinates were converted to metric coordinates (mm) based on information about the spatial resolution of the images and the arbitrarily assumed place of the beginning of the coordinate system (associated with the place where the sample is handled in a still holder).

The shape of the edge of the test sample in subsequent images of the recorded sequence is shown in Figure 7.

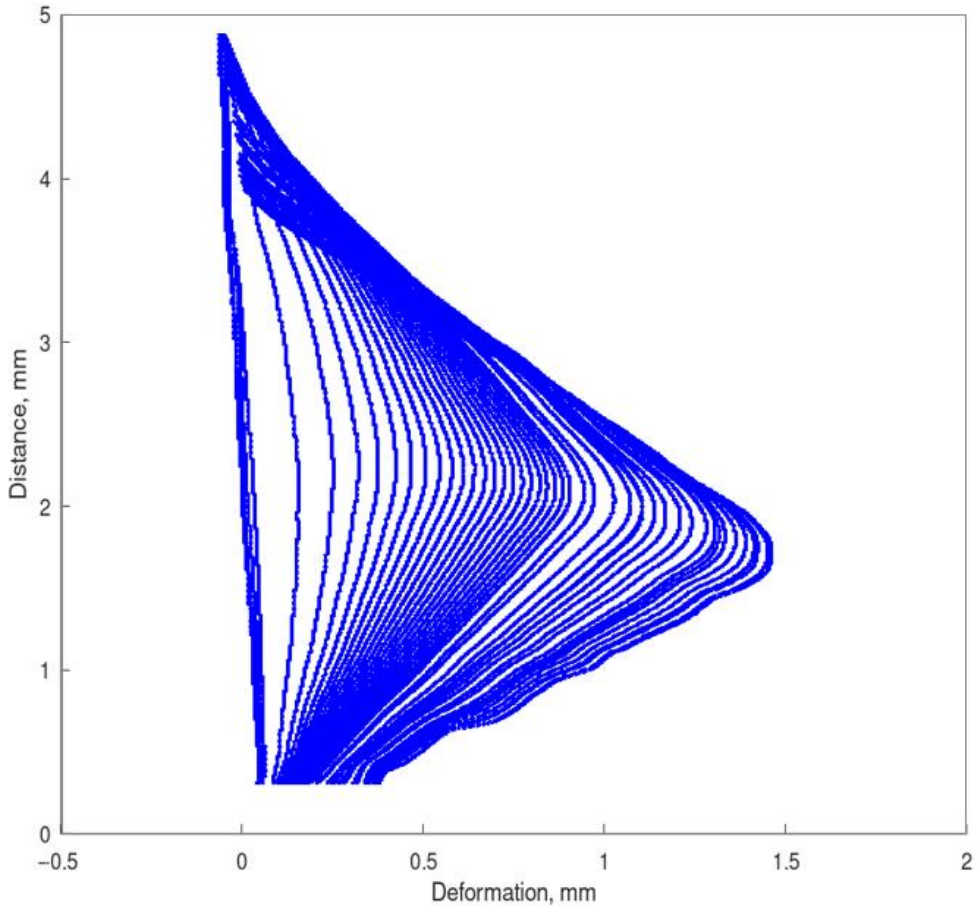

Figure 7. An example of the shape of the edge of the sample being tested in subsequent images of the recorded sequence.

The apparent movement of the lower end of the sample edge is the result of limiting the analysis field to the area of correct edge detection in the image. The assumed origin of the coordinate system, associated with the edge of the still handle, is below the bottom edge of the image.

2.4. Synchronization of Image Data and Measurement Results from the Testing Machine

The average values of the coordinates of the corners of the movable and stationary checkerboard were used to determine the displacement of the handle at the moments of recording individual photos. Based on this information, the time of photo recording as a function of the time of measurement data acquisition in the testing machine was estimated, as shown in Figure 8. The result was the synchronization of data recording times from two different sources.

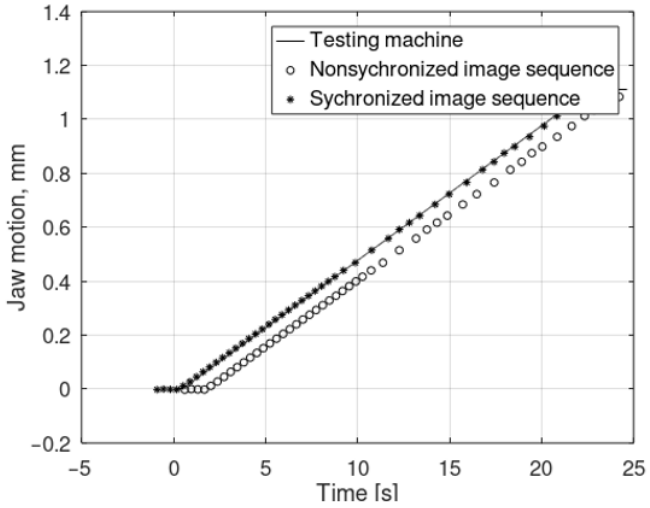

Figure 8. Displacement of the handle of the testing machine estimated from a series of images before and after synchronization with data from the machine.

2.5. Estimation of Deformation Parameters of the Tested Paper Sample

The measurement data obtained as a result of the pre-processing and analysis of the images were further analyzed in order to determine the value of so-called the deflection arrow of the paper sample and the parameters of the sinusoidal function modelling the shape of the sample edges. This is preceded by a rotation of the coordinate system of the machine to position the edge of the sample at the beginning of the test in a vertical direction. This operation is performed on the basis of the coordinates of the sample mounting in the machine holders. After this correction, the deflection arrow is defined as the difference in the horizontal coordinate of the places of attachment of the sample in the handles and the place of the greatest deflection of the sample.

The shape of the sample is then modelled using a sinusoidal function of image coordinates $x = f(y)$:

$$x = C + A \cdot sin\left(\frac{2 \cdot \pi \cdot y}{Pr} + \varphi\right), \tag{1}$$

where:

C-constant—the shift relative to the beginning of the coordinate system (it can change in subsequent photos as a result of, for example, camera vibrations, it is not important in measuring the deflection of the sample),
A—amplitude of the sine wave function modelling the deflection,
Pr—the period of the sine wave modelling the deflection (at the initial stage of measurement, before the buckling of the sample, it cannot be determined accurately),
φ—the initial phase of the sine wave modelling the deflection (not relevant from the point of view of deflection analysis, but must be a variable in order to match the model well with the measurement data).

The desired values of the parameters of the sample shape modelling function are searched in the optimization procedure that minimizes the SSE_{Sh} error between the measurement data and the modelling result. The error is described by Equation (2):

$$SSE_{Sh} = \sum_i \left(x_i - C - A \cdot \sin\left(\frac{2 \cdot \pi \cdot y_i}{Pr} + \varphi\right)\right)^2, \tag{2}$$

where:

i—index of the point at the edge of the test sample,
x_i—the horizontal coordinate of the *i*-th point at the edge of the sample,
y_i—the vertical coordinate of the *i*-th point on the edge of the sample.

2.6. An Example of Analysis of Measurement Data—Crushing a Paper Sample Subjected to the Test with a Clamping Length of 4 mm

The results of the measurements recorded during the MD crushing test of the packaging paper and the analysis of the images recorded at that time and the modelling of the sample shape using the function given by the Formula (1) are shown in Figures 8–10.

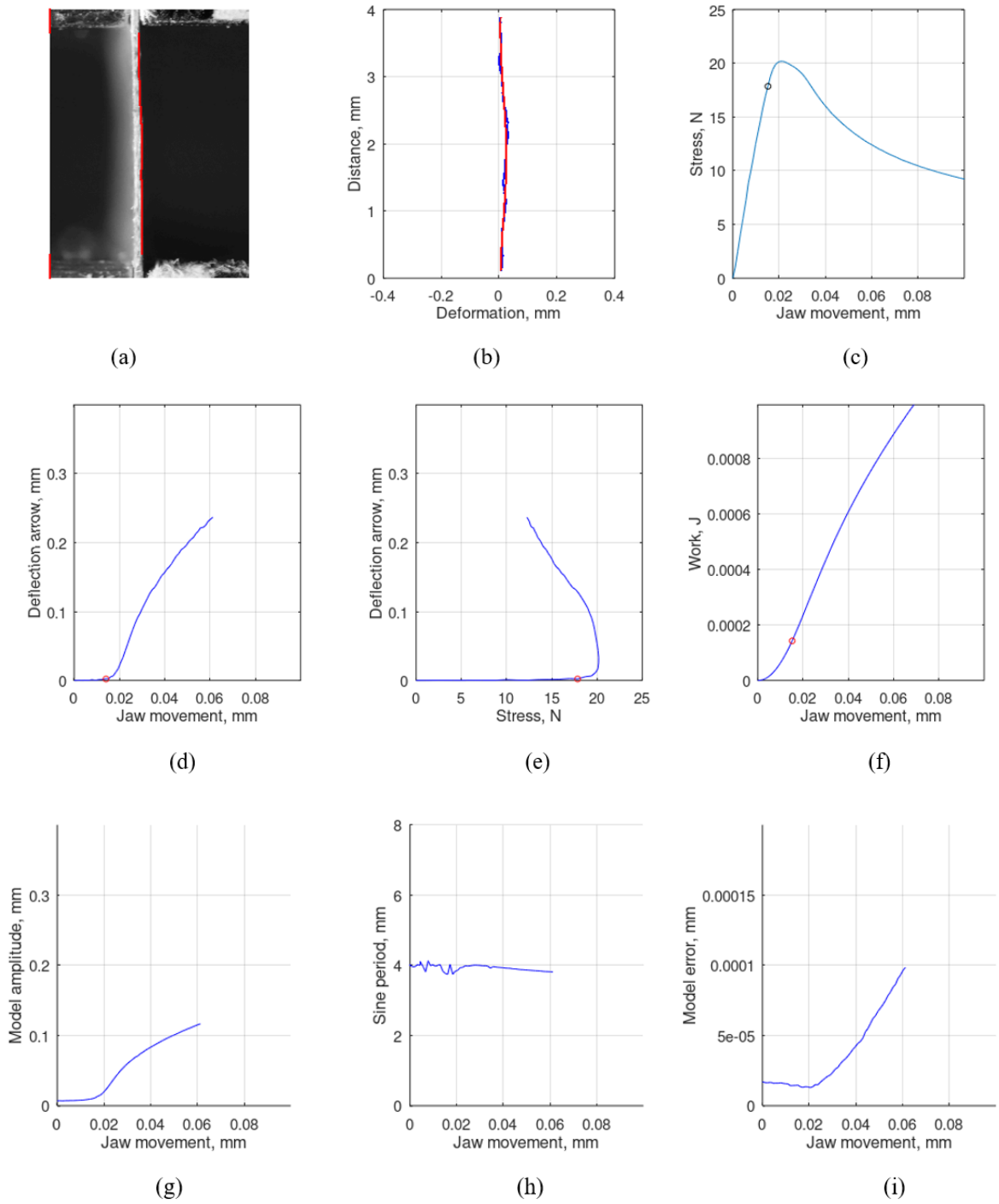

Figure 9. The results of compression analysis of a 4 mm long paper sample at the time of the appearance of the sample buckling.

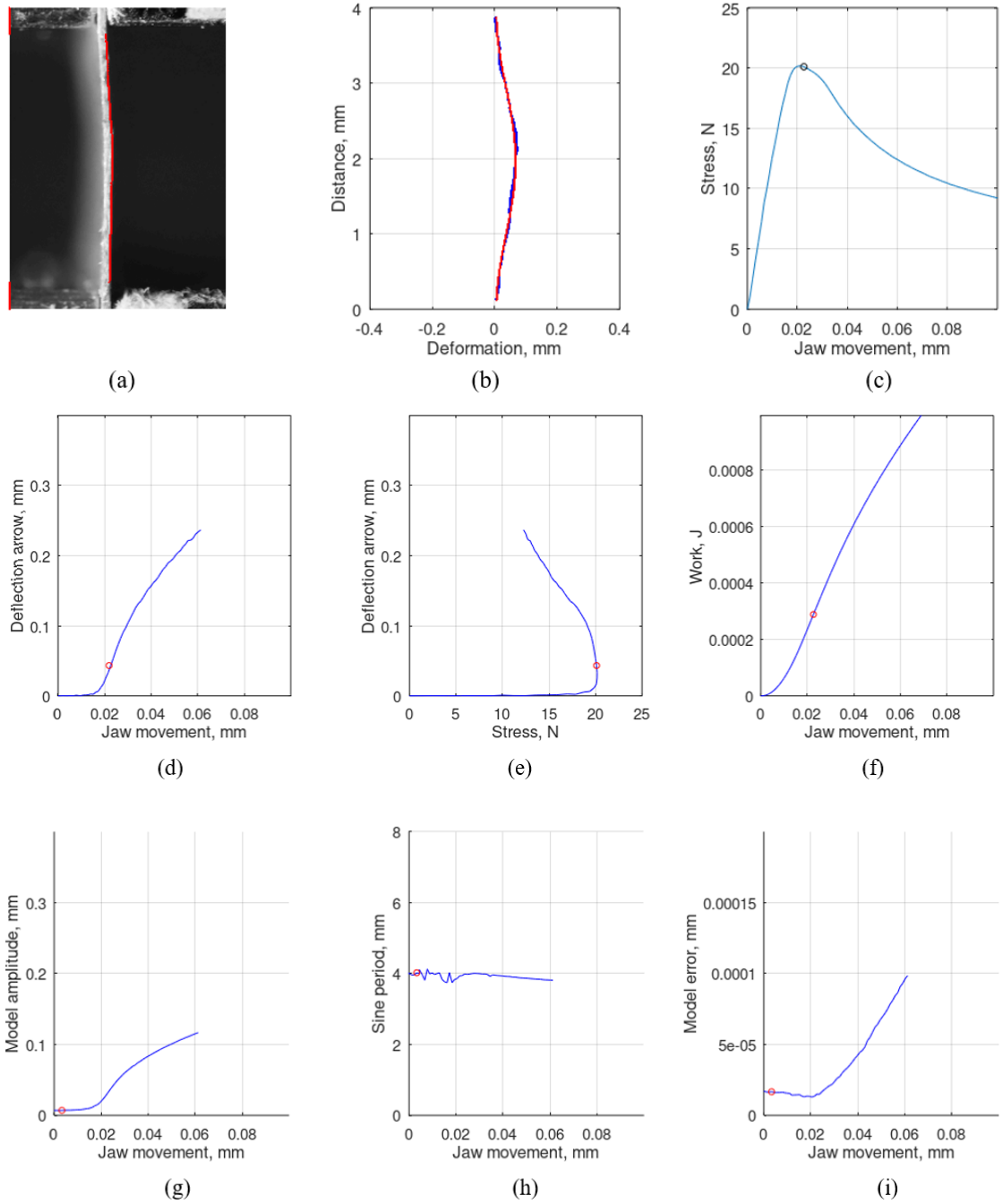

Figure 10. The results of the compression analysis of the paper sample at a clamping length of 4 mm at the maximum compressive force.

Meaning of the individual charts in each drawing:

(a)—an image of the sample with the edge detected,

(b)—the shape of the detected edge in the coordinate system determined on the basis of the indicated points of attachment of the sample,

(c)—the shape of the force curve as a function of displacement of the handle with the marked place of recording of the shown image,

(d)—the value of the deflection arrow as a function of displacement of the movable handle,

(e)—the value of the deflection arrow as a function of force,

(f)—work on deformation of the sample as a function of displacement of the handle,

(g)—the amplitude value of the sine wave function modelling the shape of the sample as a function of displacement of the handle,

(h)—the period of the sinusoidal function modelling the shape of the sample as a function of displacement of the handle,

(i)—the value of the sample shape modelling error as a function of the handle displacement.

A round, red marker on the background of curves representing individual functional dependencies shows the obtained values in the discussed phase of the compression process.

Figure 9 shows the state of the sample at the time of transition from the pure compression phase to the buckling phase of the sample. In the moments preceding this state, modelling the shape of the sample with a sinusoidal function does not make sense. Therefore, graphs from (g) to (i) in Figure 9 begin with the place marked with a dot.

Figure 10 shows the state of the sample when the maximum force is reached. Up to this point, the approximation of the shape of the sample using the function described by the Formula (1) is characterized by a small error value, which means that the buckling takes the shape of a sinusoid until the maximum force is reached.

Figure 11 shows the condition of the sample after its destruction. In this state, the approximation of the sample shape using the function described by the Formula (1) is not very accurate, as indicated by the increasing value of the modelling error. The sample takes a shape similar to two sections connecting the connection points.

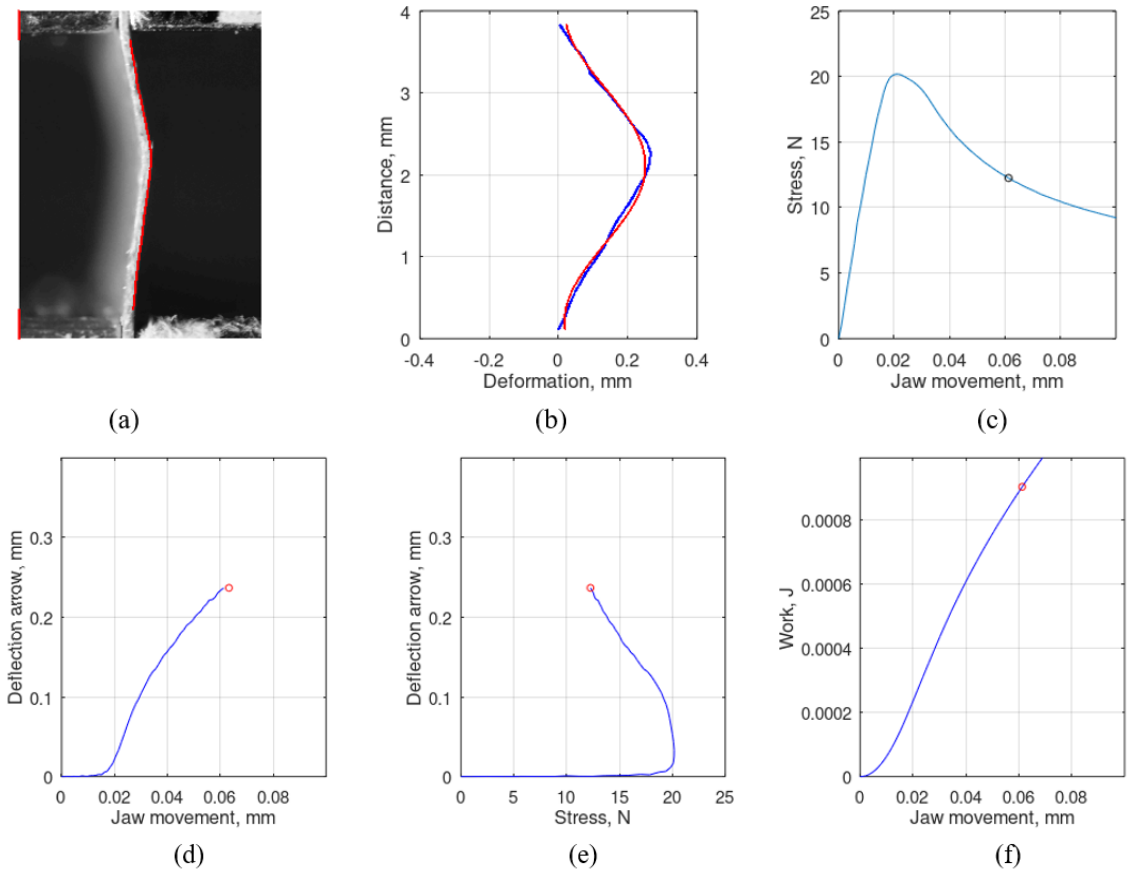

Figure 11. *Cont.*

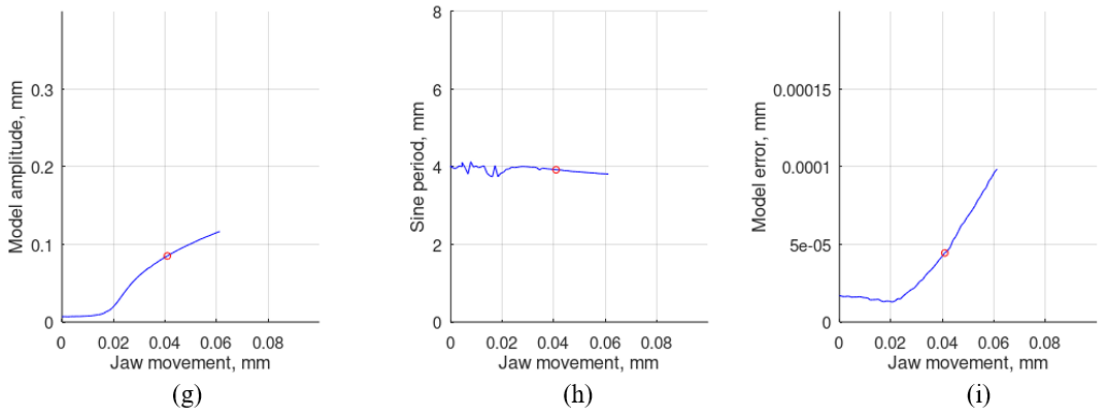

Figure 11. The results of compression analysis of a 4 mm long paper sample after breaking the sample.

3. Results

The results of measurements made with sample clamping lengths from 0.7 mm to 5 mm are presented. A measurement experiment was performed to study the behavior of samples of packaging paper crushed in the direction of MD. The sample was 15 mm wide, as in a typical SCT test. The standard clamping length in the SCT test is 0.7 mm. However, different values of the sample connection length were used: 0.7 mm, 1.3 mm, 2 mm, 3 mm, 4 mm and 5 mm. The thickness of the paper was 0.14 mm.

Figure 12 shows the shape of a curve representing the dependence of the compressive force of a paper sample on the displacement of the movable handle with fastening lengths from 0.7 mm to 5 mm.

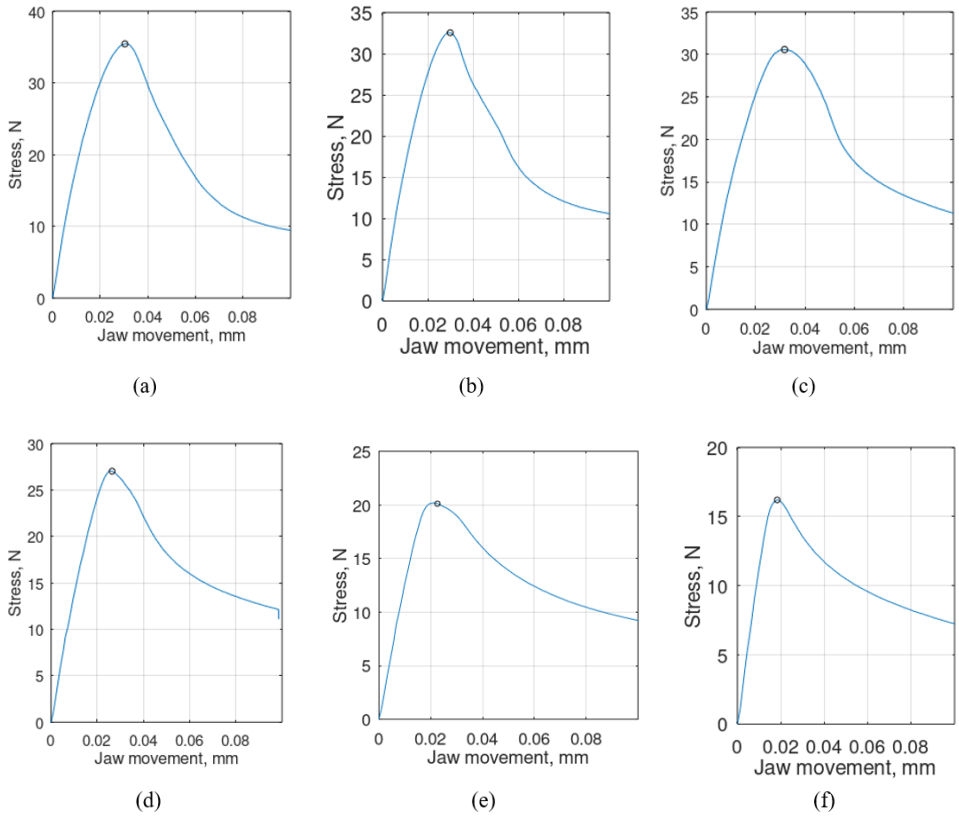

Figure 12. Shape of the dependence of the compressive force of the paper sample on the displacement of the movable handle at the fastening lengths: (**a**) 0.7 mm, (**b**) 1.3 mm, (**c**) 2 mm, (**d**) 3 mm, (**e**) 4 mm, (**f**) 5 mm.

As the length of the fastening increases, a tendency to decrease the maximum force occurring during the test is observed. Curves for a length of 0.7–5 mm increase rapidly until the maximum value is reached, and then fall sharply, but with a smaller gradient. Table 1 shows the maximum values of the compressive force as a function of the clamping length.

Table 1. Dependence of the maximum value of the compressive force on the connection length.

Connection Length, mm	0.7	1.3	2.0	3.0	4.0	5.0
Maximum value of compressive force, N	35.42	32.57	30.56	27.04	20.17	16.20

At the same time, it can be seen in Figure 13a–c that with fastening lengths of less than 3 mm at the moment of reaching the maximum force no buckling is observed. With longer lengths of fastening, the buckling has the shape of a sinusoid fragment.

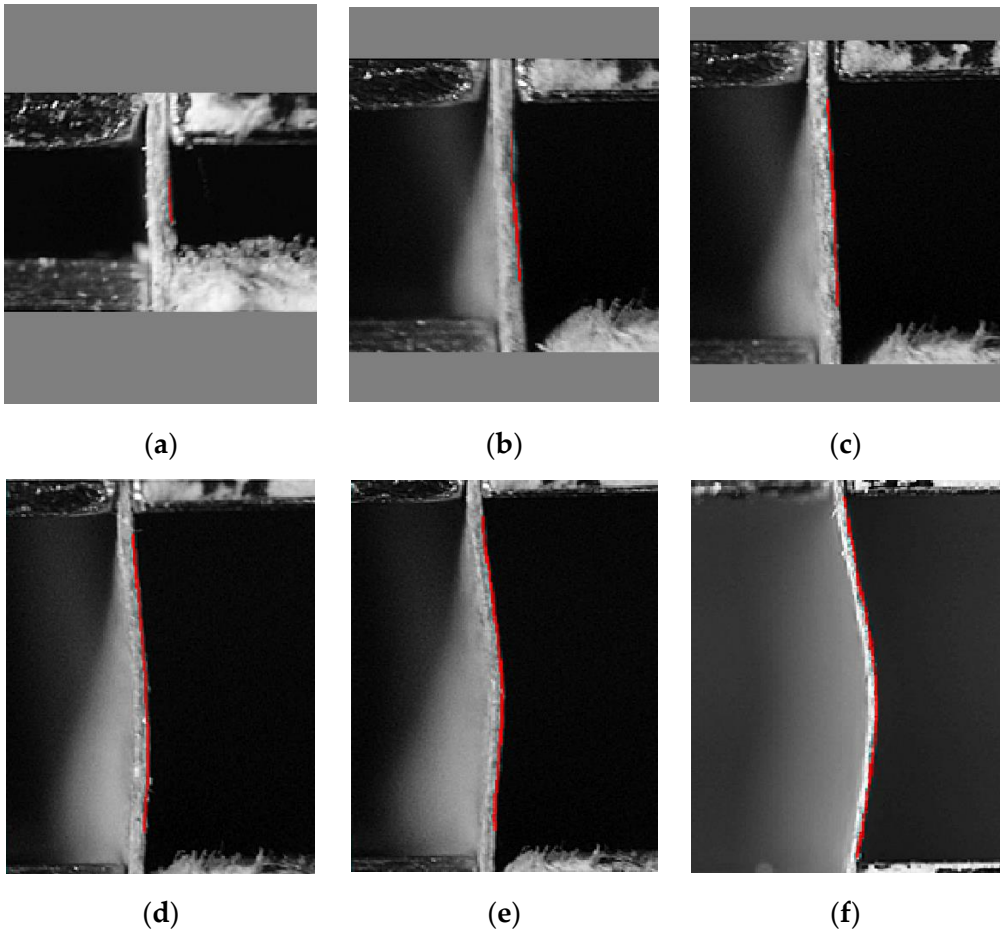

Figure 13. Shape of the edge of the compressed paper sample when the maximum force is reached at the clamping lengths: (**a**) 0.7 mm, (**b**) 1.3 mm, (**c**) 2 mm, (**d**) 3 mm, (**e**) 4 mm, (**f**) 5 mm.

Figure 14 shows the shape of the samples compressed at the time of destruction for the plug-in lengths to be analyzed.

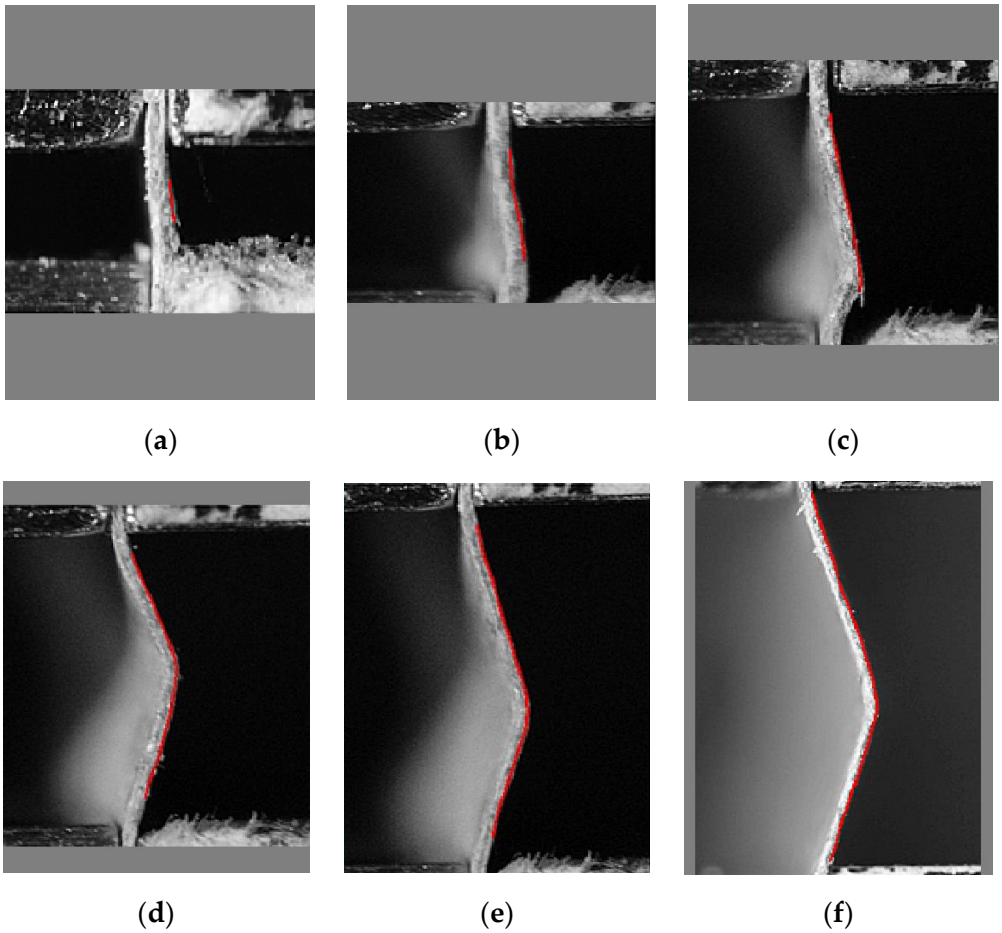

Figure 14. Shape of the edges of the compressed samples at the time of destruction for the connection length: (**a**) 0.7 mm, (**b**) 1.3 mm, (**c**) 2 mm, (**d**) 3 mm, (**e**) 4 mm, (**f**) 5 mm.

4. Discussion

The results of the measurements made it possible to draw a number of conclusions. For a length of 0.7 mm, the paper fibers delaminated and crushed near the fixed lower handle of the machine. In this case, the ratio of the length of the sample to its thickness is L/g = 5. For lengths of 1.3 and 2.0 mm, destruction shall also occur near the lower handle with visible horizontal displacement of the samples. For these cases, we have L/g = 9.3 and L/g = 14.3, respectively. For the fastening lengths of 3.0 (L/g = 21.4) and 4.0 mm (L/g = 28.5), the destruction of the samples takes place in the central part and the sample takes the shape of the letter V. Note that paper edges enter tangentially into both handles. However, for a length of 5 mm (L/g = 35.7), the V-shape is very clearly visible, in particular the refraction itself. The sample at the places of attachment to both handles takes the shape as for joint-like support.

In the theory of thin-walled structures, the following classification is assumed: when L/g > 25–30, where L is a smaller overall dimension, the plates are thin-walled; when 5 < L/g < 25 the plates are of medium thickness, while L/g $\leq$ 5 the plates are thick [16,17]. According to this classification, the clamping length L = 0.7 mm corresponds to thick plates, and for L = 1.3, 2.0, 3.0, 4.0 plates of medium length, and for L = 5.0 thin plate. For plates of medium thickness, modifications are made in relation to thin plates [18,25,26].

Figure 15 shows diagrams of changes in the deflection arrow of the sample as a function of displacement of the movable handle of the testing machine with the place where the maximum force is reached.

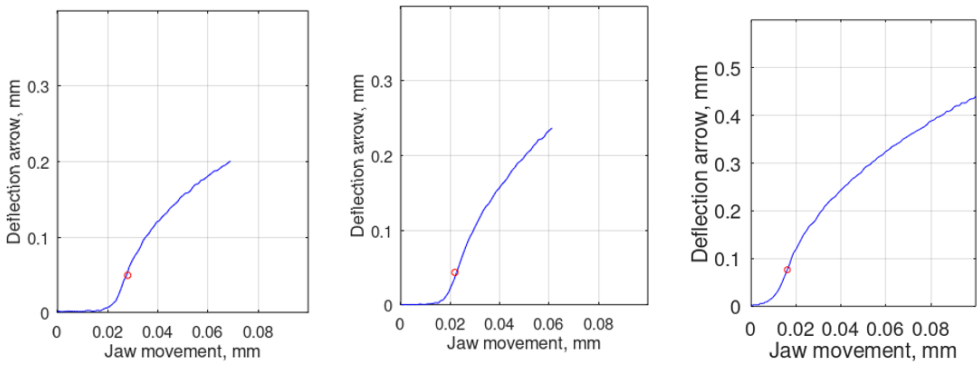

Figure 15. Dependence of the value of the deflection arrow on the displacement of the movable handle at the fastening lengths: (**a**) 3 mm, (**b**) 4 mm, **(c)** 5 mm.

The correctness of determining the deflection arrow using the developed image analysis technique was checked by comparing measured sample shortening with the analytically determined value using the formula given in [16]:

$$\Delta l = l\left(1 - \sqrt[2]{1 - \left(\frac{2\delta}{l}\right)^2}\right) \tag{3}$$

where:

l—sample length
Δl—sample shortening
δ—deflection arrow.

Figure 16 shows a comparison of the measured and theoretically calculated shortening of the paper sample with a clamping length of 4 mm and 5 mm as a function of its deflection. A slight difference between the measured and calculated values may result from the adopted destruction model, which does not reflect all the phenomena occurring during the test, or the inaccuracy of determining the deflection arrow by imaging methods.

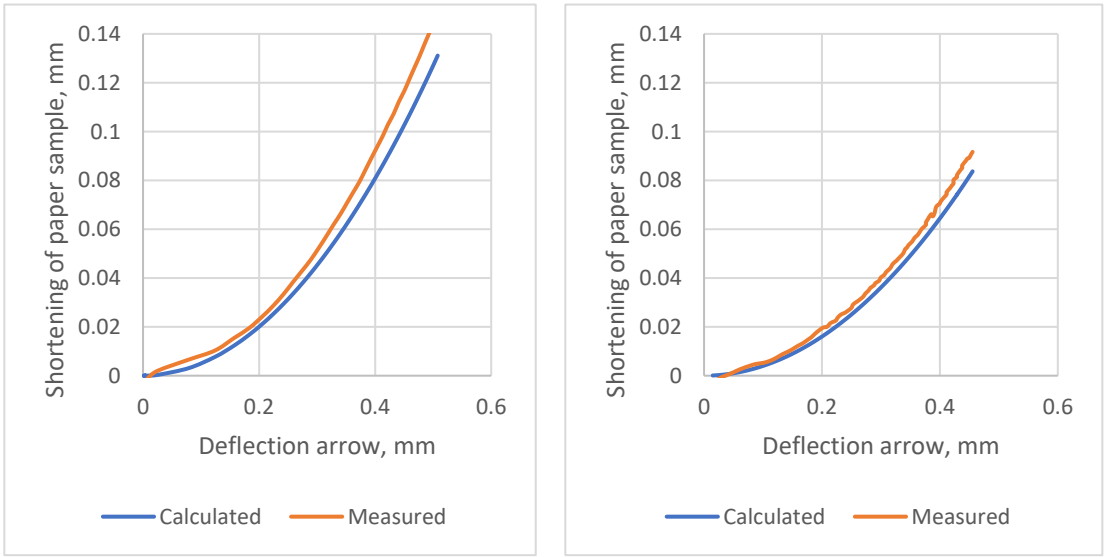

Figure 16. Comparison of the measured and theoretically calculated sample shortening during the test for clamping length of (**a**) 4 mm and (**b**) 5 mm.

Figure 17 summarizes the diagrams of changes in the period of the sinusoidal function approximating the shape of the test sample as a function of displacement of the movable handle of the testing machine. Estimating the period until buckling occurs is not justified, since the shape of the edge of the sample does not resemble a sinusoid. From the moment the maximum force is reached, the value of the period stabilizes at a level comparable to the length of the fastening.

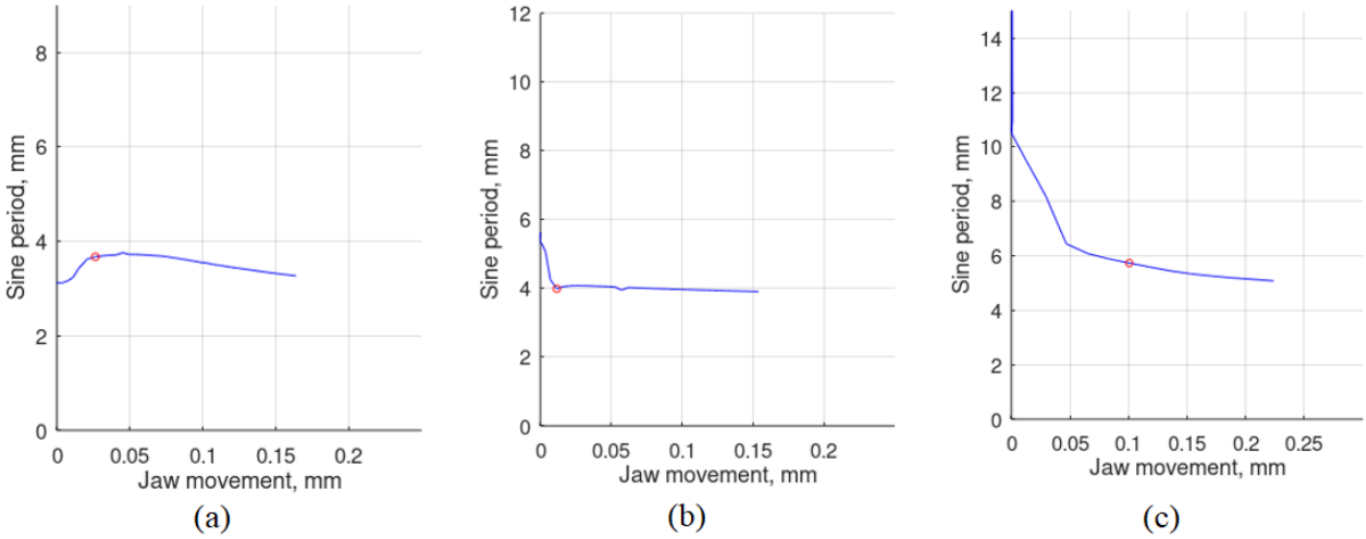

Figure 17. Dependence of the period of the sine wave modelling the shape of the sample on the displacement of the movable handle at the lengths of fastening: (**a**) 3 mm, (**b**) 4 mm, (**c**) 5 mm.

5. Conclusions

A measurement technique was developed, based on the simultaneous measurement of the dependence of the compressive force on the displacement of the movable handle of a universal testing machine and the recording of a series of images of a compressed sample of the tested material. This technique has a number of advantages over the traditional approach of recording only jaw movement and the force curve during the test. It enables non-contact measurement of the value of the deflection arrow of the sample during the test and gives the opportunity to observe its shape. This allows the shape of the tested paper samples to be modelled with different curves, e.g., a sinusoidal function. Thanks to this, it becomes possible to determine the relationship between the deflection arrow and other variables, e.g., force, displacement of the handle of the testing machine or work carried out on the sample.

Visualization of changes in the shape of the sample in subsequent phases of the test together with the quantities measured using a universal testing machine facilitates the prediction of the model of destruction under given conditions and gives the possibility of its quantitative verification by determining the modelling error of the shape itself or the parameters determined on its basis. As an example of such a possibility, the effects of approximating the shape of the sample using the sinusoidal function and the error graph of this approximation allowing to estimate the limits of applicability of the proposed model are shown. The development of a model of paper destruction during compression is of great importance for predicting the strength properties of corrugated board and cardboard packaging produced from it. This will allow for savings in terms of packaging products in transport and reducing the consumption of paper raw materials for the production of cardboard.

In order for the developed measurement technique to be fully useful in testing the strength properties of paper, the process of registration and pre-processing of sample images must be optimized. In particular, the procedure used to detect the optical edge of the sample does not allow for its correct detection in the vicinity of the attachment to

the UTM holder. It is planned to mask the handle with black stickers. The authors are also looking for optimal image size settings, which will maximize the number of images recorded during the examination. Further research is also planned to develop an analytical model describing the phenomena occurring during paper compression and methods for determining the mechanism of paper destruction and the corresponding maximum force that destroys a paper sample.

Author Contributions: Conceptualization, W.S.; methodology, W.S. and P.P.; software, P.P.; validation, P.P. and M.B.; formal analysis, Z.K.; investigation, Z.K.; resources, M.B.; data curation, M.B. and P.P.; writing—original draft preparation, P.P., Z.K. and W.S.; writing—review and editing, P.P., W.S., M.B. and Z.K.; visualization, P.P.; supervision, W.S.; project administration, W.S. All authors have read and agreed to the published version of the manuscript.

Funding: This research received no external funding.

Institutional Review Board Statement: Not applicable.

Informed Consent Statement: Not applicable.

Data Availability Statement: The data presented in this study are available on request from the corresponding author. The data is not publicly available due to the high degree of complexity of their organization. The authors have not yet developed an appropriate standard for their storage.

Conflicts of Interest: The authors declare no conflict of interest.

References

1. Rzepa, S. Parametry papieru. In Proceedings of the Sympozjum Mondi Packaging "From Fibre to Corrugated Board", Świecie, Poland, 1–2 December 2004.
2. Bai, J.; Wang, J.; Pan, L.; Lu, L.; Lu, G. Quasi-static axial crushing of single wall corrugated paperboard. *Compos. Struct.* **2019**, *226*, 111237. [CrossRef]
3. Czechowski, L.; Bieńkowska, M.; Szewczyk, W. Paperboard tubes failure due to lateral compression—Experimental and numerical study. *Compos. Struct.* **2018**, *203*, 132–141. [CrossRef]
4. Kołakowski, Z.; Szewczyk, W.; Bieńkowska, M.; Czechowski, L. New method for evaluation of radial crush strength of paper cores. *Mechanika* **2018**, *24*, 169–173. [CrossRef]
5. Gajewski, T.; Garbowski, T.; Staszak, N.; Kuca, M. Crushing of double-walled corrugated board and its influence on the load capacity of various boxes. *Energies* **2021**, *14*, 4321. [CrossRef]
6. Yu-Ping, E.; Wang, Z.-W. Plateau stress of paper honeycomb as response to various relative humidities. *Packag. Technol. Sci.* **2010**, *23*, 203–216. [CrossRef]
7. Abbès, B.; Guo, Y.Q. Analytic homogenization for torsion of orthotropic sandwich plates: Application to corrugated cardboard. *Compos. Struct.* **2010**, *92*, 699–706. [CrossRef]
8. Semple, K.E.; Sam-Brew, S.; Deng, J.; Cote, F.; Yanm, N.; Chen, Z.; Smith, G.D. Properties of commercial Kraft paper honeycomb furniture stock panels conditioned under 65 and 95 percent relative humidity. *For. Prod. J.* **2015**, *65*, 106–122. [CrossRef]
9. Kmita-Fudalej, G.; Szewczyk, W.; Kołakowski, Z. Calculation of honeycomb paperboard resistance to edge crush test. *Materials* **2020**, *13*, 1706. [CrossRef] [PubMed]
10. Fadiji, T.; Ambaw, A.; Coetzee, C.J.; Berry, T.M.; Opara, U.L. Application of finite element analysis to predict the mechanical strength of ventilated corrugated paperboard packaging for handling fresh produce. *Biosyst. Eng.* **2018**, *174*, 260–281. [CrossRef]
11. Li, X.; Wang, J.; Chuang, C.; Gao, D.; Lu, G.; Lu, L.; Wang, Z. Mathematical models for predicting the quasi-static stress characteristics of corrugated paperboard with sinusoidal core along the longitudinal compression. *Int. J. Mech. Sci.* **2018**, *149*, 136–149. [CrossRef]
12. Kubiak, T.; Kolakowski, Z.; Swiniarski, J.; Urbaniak, M.; Gliszczynski, A. Local buckling and post-buckling of composite channel-section beams—Numerical and experimental investigations. *Compos. Part B* **2016**, *91*, 176–188. [CrossRef]
13. Mou, X.-N.; Lu, L.-X.; Zhou, Y.-L. Evaluation of in-plane compressive densification strain of honeycomb paperboard. *Adv. Mech. Eng.* **2020**, *12*, 1–11. [CrossRef]
14. Smardzewski, J.; Prekrat, S. Modelling of thin paper honeycomb panels for furniture. In Proceedings of the International Conference Ambienta, Wood is Good—With Knowledge and Technology to a CompetitiveForestry and Wood Technology Sector, Zagreb, Croatia, 12 October 2012; pp. 179–186.
15. *PN-EN ISO 3035: 2011*; Tektura Falista Oznaczanie Odporności na Zgniatanie Płaskie. Polski Komitet Normalizacyjny: Warsaw, Poland, (Polish Standard); 2011.
16. Murray, N.W.; Khoo, P.S. Some basic plastic mechanism in the local buckling of thin-walled steel structures. *Int. J. Mech. Sci.* **1981**, *23*, 703–713. [CrossRef]

17. Królak, M. (Ed.) *Stany Zakrytyczne i Nośność Graniczna Cienkościennych Dźwigarów o Ścianach Płaskich (Critical States and Ultimate Capacity of Thin-Walled Girders with Flat Walls)*; PWN, Warszawa-Łódź: Daimlera, Poland, 1990.
18. Reddy, J.N. *Mechanics of Laminated Composite Plates and Shells: Theory and Analysis*, 2nd ed.; CRC Press: Boca Raton, FL, USA, 2004. [CrossRef]
19. Bin Kamarudin, M.N.; Mohamed Ali, J.S.; Aabid, A.; Ibrahim, Y.E. Buckling Analysis of a Thin-Walled Structure Using Finite Element Method and Design of Experiments. *Aerospace* **2022**, *9*, 541. [CrossRef]
20. Gonzalez, R.C.; Woods, R.E. *Digital Image Processing*, 3rd ed.; Prentice Hall, SE: Hoboken, NJ, USA, 2007; ISBN 978-0-13-168728-8.
21. Pełczyński, P.; Szewczyk, W.; Bieńkowska, M. Single-Camera System for Measuring Paper Deformations Based on Image Analysis. *Metrol. Meas. Syst.* **2021**, *28*, 509–522. [CrossRef]
22. Considine, J.M.; Scott, C.T.; Gleisner, R.; Zhu, J.Y. Use of digital image correlation to study the local deformation field of paper and paperboard. In Proceedings of the 13th Fundamental Research Symposium, Cambridge, UK, 11–16 September 2005; pp. 613–630.
23. Stanier, S.A.; Blaber, J.; Take, W.A.; White, D.J. Improved image-based deformation measurement for geotechnical applications. *Can. Geotech. J.* **2016**, *53*, 727–739. [CrossRef]
24. Online; Procemex Machine Vision Applications in Pulp and Paper Industry Offer Different Solutions for Pulp Furnish, Pulp bale, and Roll Quality Inspection. Available online: https://www.procemex.com/machine-vision-applications (accessed on 7 January 2023).
25. Volmir, A.S. *Nonlinear Dynamics of Plates and Shells*; Science Publishing House: Moscow, Russia, 1972; p. 432. (In Russian)
26. Kolakowski, Z.; Jankowski, J. Some inconsistencies in the nonlinear buckling plate theories—FSDT, S-FSDT, HSDT. *Materials* **2021**, *14*, 2154. [CrossRef]